Opto-Electronic Science

Supplementary information

April 2024, Vol. 3, No. 4

DOI: 10.29026/oes.2024.230036

High-intensity spatial-mode steerable frequency up-converter toward on-chip integration

Haizhou Huang[2], Huaixi Chen[2]*, Huagang Liu[1,3], Zhi Zhang[1], Xinkai Feng[4], Jiaying Chen[1,5], Hongchun Wu[1,5], Jing Deng[1,5], Wanguo Liang[1]* and Wenxiong Lin[1,3]*

[1]Key Laboratory of Optoelectronic Materials Chemistry and Physics, Fujian Institute of Research on the Structure of Matter, Chinese Academy of Science, Fuzhou 350002, China; [2]Key Laboratory of Opto-Electronic Science and Technology for Medicine of Ministry of Education, Fujian Provincial Key Laboratory of Photonics Technology, College of Photonic and Electronic Engineering, Fujian Normal University, Fuzhou 350117, China; [3]Fujian Science & Technology Innovation Laboratory for Optoelectronic Information of China, Fuzhou 350108, China; [4]College of Digital Economy, Fujian Agriculture and Forestry University, Fuzhou 350002, China; [5]University of Chinese Academy of Sciences, Beijing 100049, China.

*Correspondence: chenhx@fjnu.edu.cn; wgl@fjirsm.ac.cn; wxlin@fjirsm.ac.cn

This file includes:

Section 1: Spatial modes of the ridge waveguide
Section 2: Calculating the inter-mode quasi-phase matching efficiency
Section 3: Device fabrication and characterization
Section 4: Experimental details
Section 5: Evaluating the coupling modes
Section 6: Wavelength-dependent spatial mode steering scheme

Supplementary information for this paper is available at https://doi.org/10.29026/oes.2024.230036

Section 1: Spatial modes of the ridge waveguide

For the Z-cut PPMgLN waveguide in Fig. 1(a), spatial modes inside the waveguide were calculated using COMSOL Multiphysics Software using the frequency domain module for electromagnetic waves. The effective indices of the PPLN waveguide at a broad temperature range can be calculated synchronously for the pump, signal, and SFG lights. Here, temperature-dependent Sellmeier formula of the LN crystal was used [S1]:

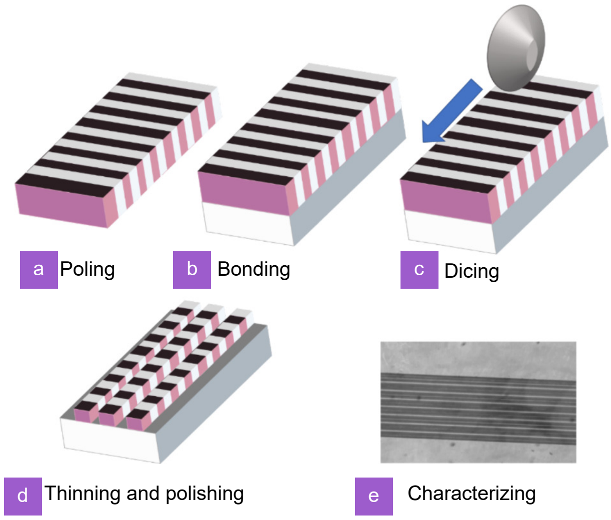

Fig. S1 | Flowchart for preparing the spatial-mode steerable SFG waveguide.

$$n_e(T) = \sqrt{A_{e1} + fB_{e1} + \frac{A_{e2} + fB_{e2}}{\lambda^2 - (A_{e3} + fB_{e3})^2} + \frac{A_{e4} + fB_{e4}}{\lambda^2 - A_{e5}^2} - A_{e6}\lambda^2}\ , \quad \text{(S1)}$$

where $f(T) = (T\text{-}24.5)(T+570.82)$, and parameters from A_{e1} to A_{e6} and B_{e1} to B_{e2} are listed in Table S1.

Table S1 | Sellmeier parameters for the LN crystal

A_{e1}	A_{e2}	A_{e3}	A_{e4}	A_{e5}	A_{e6}
5.756	0.0983	0.2020	189.32	12.52	$1.32*10^{-2}$
B_{e1}	B_{e2}	B_{e3}	B_{e4}		
$2.86*10^{-6}$	$4.7*10^{-8}$	$6.113*10^{-8}$	$1.516*10^{-4}$		

Table S2 | Typical spatial modes among the 11 TM modes of the 1552.6-nm signal light at 25°C

Signal light

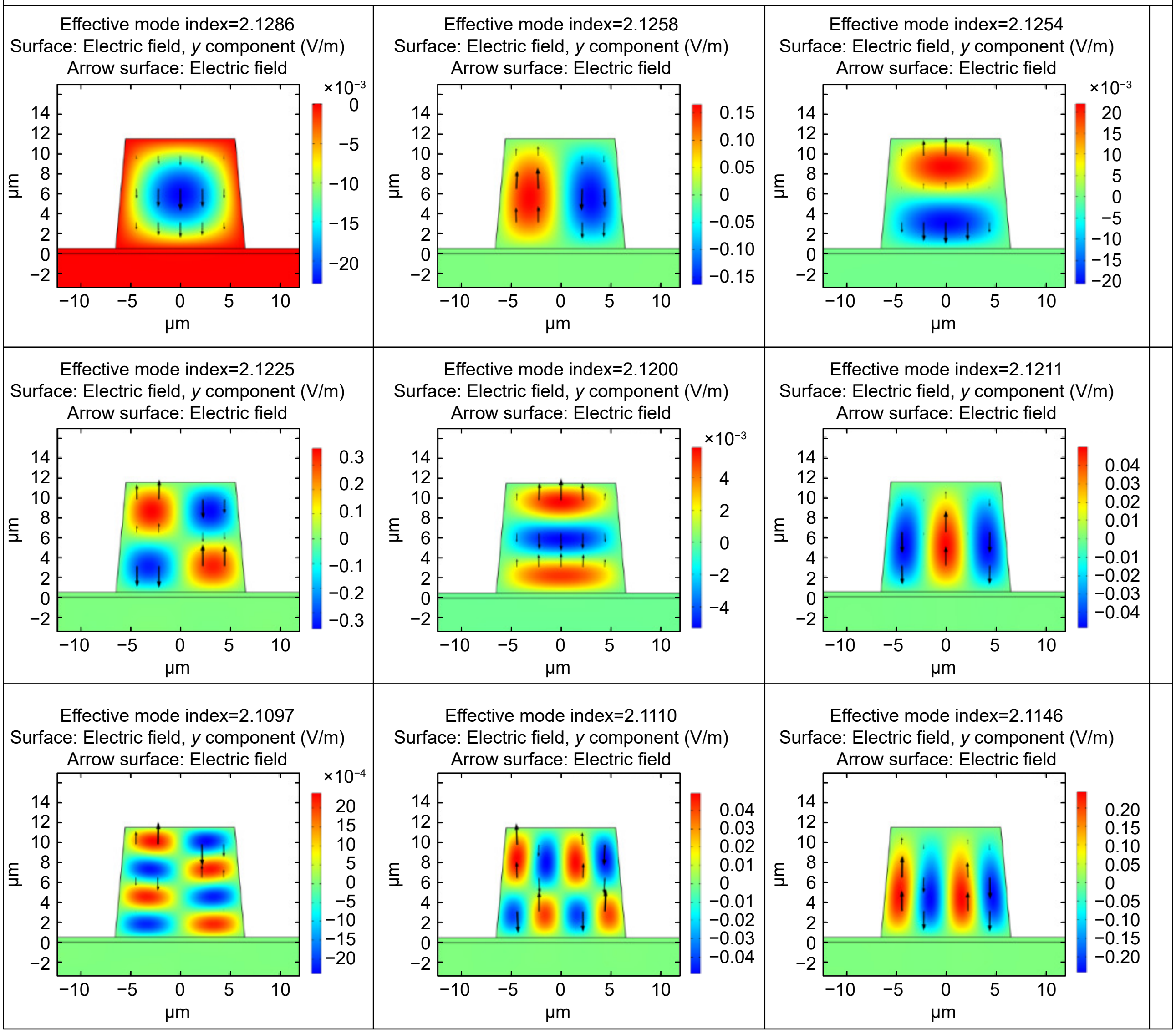

Table S3 | Typical spatial modes among the calculated 47 TM modes of the 973.85-nm pump light at 25°C

Pump light		
Effective mode index=2.1525 Surface: Electric field, *y* component (V/m) Arrow surface: Electric field 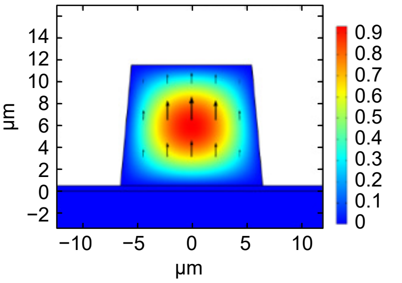	Effective mode index=2.1513 Surface: Electric field, *y* component (V/m) Arrow surface: Electric field 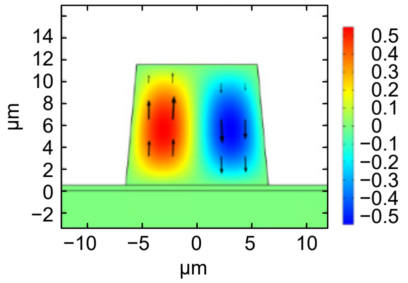	Effective mode index=2.1512 Surface: Electric field, *y* component (V/m) Arrow surface: Electric field 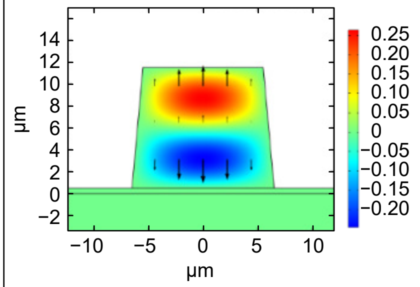
Effective mode index=2.1501 Surface: Electric field, *y* component (V/m) Arrow surface: Electric field 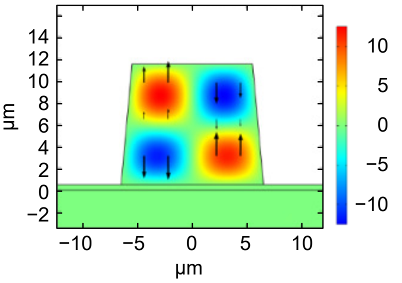	Effective mode index=2.1491 Surface: Electric field, *y* component (V/m) Arrow surface: Electric field 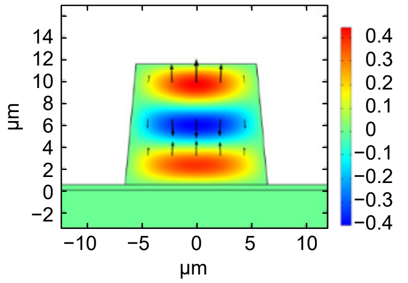	Effective mode index=2.1495 Surface: Electric field, *y* component (V/m) Arrow surface: Electric field 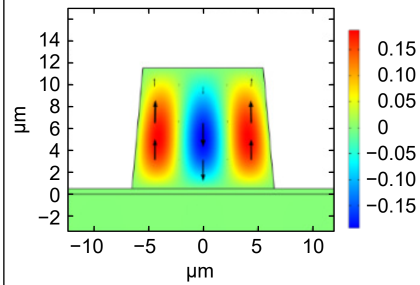
Effective mode index=2.1480 Surface: Electric field, *y* component (V/m) Arrow surface: Electric field 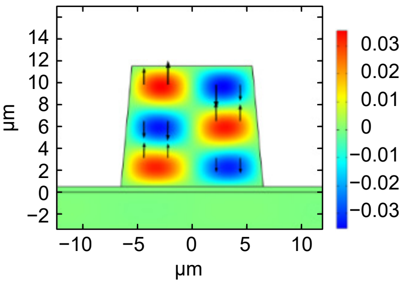	Effective mode index=2.1377 Surface: Electric field, *y* component (V/m) Arrow surface: Electric field 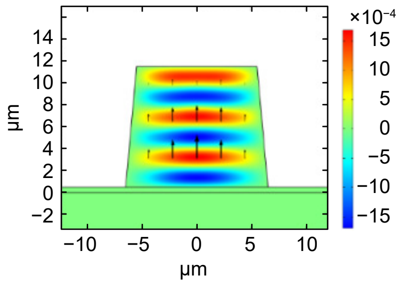	Effective mode index=2.1397 Surface: Electric field, *y* component (V/m) Arrow surface: Electric field 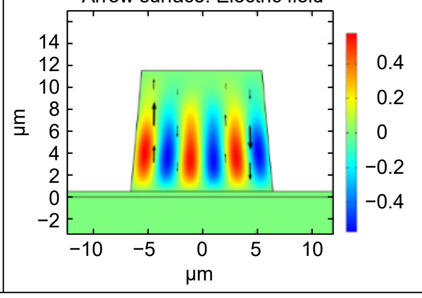

Table S4 | Typical spatial modes among the calculated 50 TM modes of the 598.47-nm SFG light at 25°C

SFG light

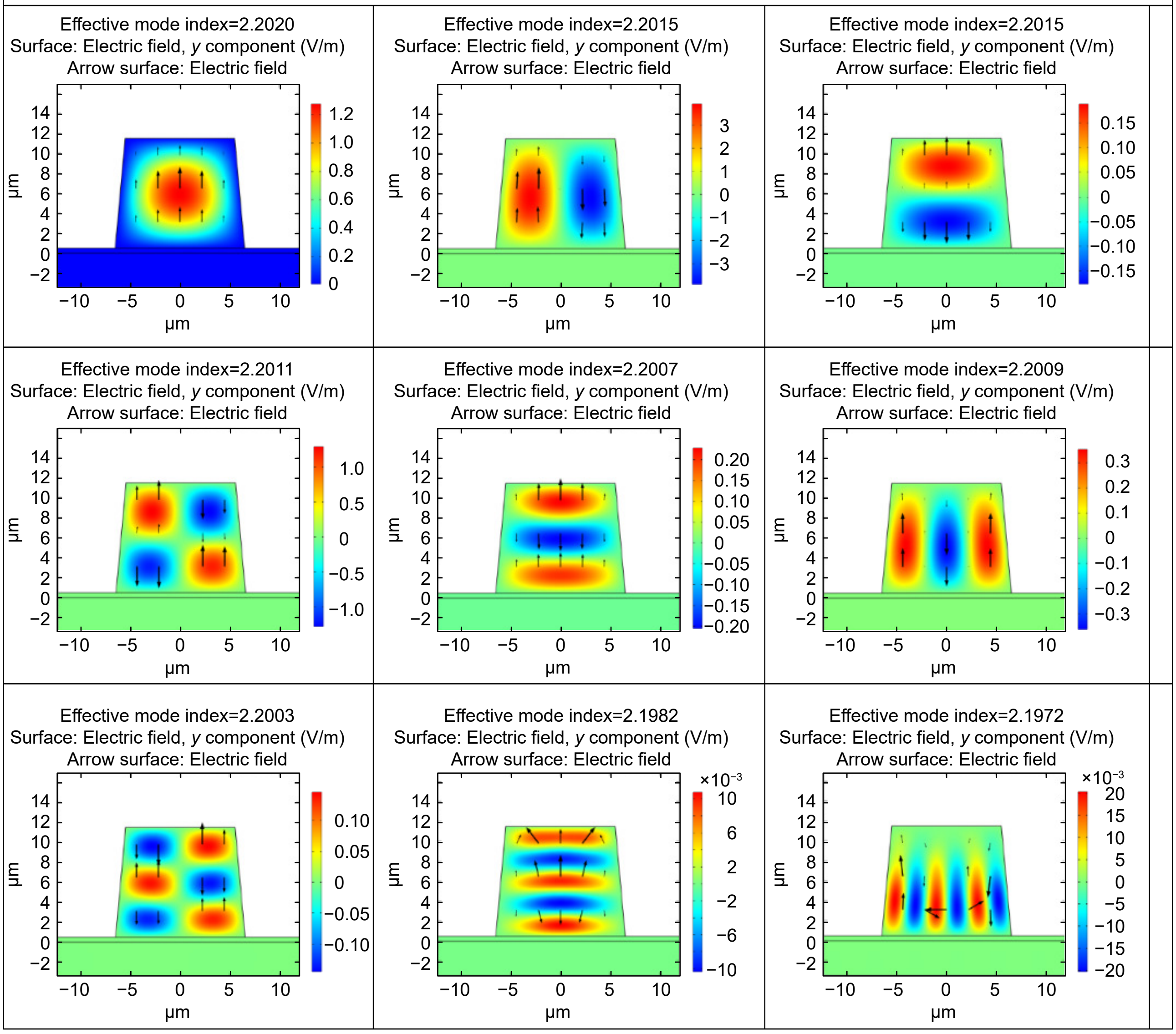

Section 2: Calculating the inter-mode quasi-phase matching efficiency

Combination of the guided signal, pump, and SFG lights can be defined as follows:

$$A_i(x,y,z)=\sum_{\mu\nu} A_i^{\mu\nu}(z)\varphi_i^{\mu\nu}(x,y)\exp(-\mathrm{i}\beta_i^{\mu\nu}z)\ , \tag{S2}$$

where i = P, S, and F denote the pump, signal, and SFG lights, respectively, and $\varphi^{i\mu\nu}$ defines the spatial profile of mode $\mu\nu$. Since the signal and pump lights are with high incident powers which are approximately un-depleted during SFG[S2], the amplitude of the SFG light at existing plane of the waveguide is expressed as follows:

$$A_{\mathrm{F}}(x,y,L)=\frac{4\pi L\mathrm{i}d_{\mathrm{eff}}A_{\mathrm{P}}A_{\mathrm{S}}}{n_{\mathrm{F}}\lambda_{\mathrm{F}}}\left(\frac{\exp(\mathrm{i}\Delta kL)-1}{\mathrm{i}\Delta kL}\right)\ , \tag{S3}$$

For $I_i = 2n_i\varepsilon_0 c|A_i|^2$, the SFG intensity is as follows:

$$I_{\mathrm{F}}(x,y,L)=\frac{8\pi^2L^2d_{\mathrm{eff}}^2I_{\mathrm{P}}^2I_{\mathrm{S}}^2}{n_{\mathrm{F}}n_{\mathrm{S}}n_{\mathrm{P}}\varepsilon_0 c\lambda_{\mathrm{F}}^2}\mathrm{sinc}^2\left(\frac{\Delta kL}{2}\right)\ , \tag{S4}$$

The power of the SFG light could be calculated by integrating Eq. S4 over the waveguide cross-section. Considering the inter-mode conversation, overlap integral Φ among modes λ_S^{ml}, λ_P^{uv}, and λ_F^{jk} at temperature T was introduced:

$$\Phi(x,y,T)=\frac{\left|\iint E_S^{ml}(x,y,T)E_P^{uv}(x,y,T)E_F^{jk*}(x,y,T)\mathrm{d}x\mathrm{d}y\right|^2}{\iint |E_S^{ml}(x,y,T)|^2\mathrm{d}x\mathrm{d}y\iint |E_P^{uv}(x,y,T)|^2\mathrm{d}x\mathrm{d}y\iint \left|E_F^{jk*}(x,y,T)\right|^2\mathrm{d}x\mathrm{d}y}\ . \tag{S5}$$

Here, E_S^{ml}, E_P^{uv}, and E_F^{jk} denote the amplitudes of the electric field y component (TM component) for modes λ_S^{ml}, λ_P^{uv}, and λ_F^{jk}, respectively, at temperature T, and the SFG power for λ_F^{jk} can be revised as follows:

$$P_F^{jk}(x,y,T)=\frac{8\pi^2L^2d_{\mathrm{eff}}^2P_P^{uv}P_S^{ml}}{n_S^{ml}n_P^{uv}n_F^{ik}\varepsilon_0 c\lambda_F^2}\Phi(x,y,T)\mathrm{sinc}^2\left(\frac{\Delta kL}{2}\right)\ . \tag{S6}$$

Section 3: Device fabrication and characterization

First, the poling period was fabricated in a 500-μm-thick Z-cut MgO: LN wafer using the standard applied pulsed voltage polarization technique (Fig. S1(a)). Next, the PPLN crystal was bonded to a 500-μm-thick LT substrate, with the assistance of a 0.5-μm-thick SiO_2 layer (Fig. S1(b)). A diamond saw was used to dice and remove the additional material (Fig. S1(c)) to form a 30-mm long PPLN waveguide array consisting of seven waveguides (Fig. S1(f)), after thinning and fine polishing (Fig. S1(d)).

A 3D profiler (S neox, Sensofar Inc., Spain) was used to characterize the detailed structure of the waveguide array and the poling period. The attenuation coefficient of each waveguide was detected by measuring the contrast of Fabry–Perot resonances with a tunable lasing system at the C-band (Fig. S2), where the third waveguide with the lowest loss of 0.29 dB/cm was used for demonstrating spatial mode steering experiments.

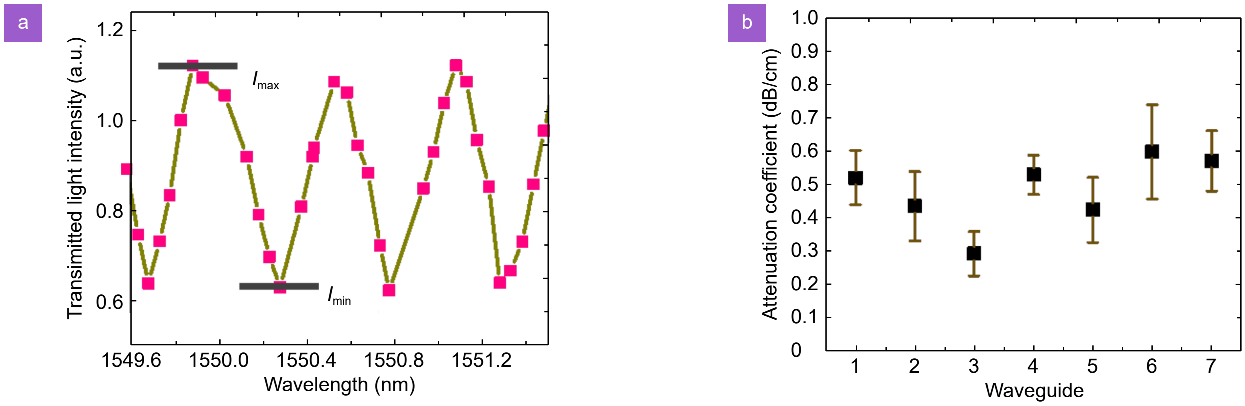

Fig. S2 | Attenuation loss of the prepared waveguide array. (**a**) Measured transmitted intensity by varying incident wavelength of the C-band laser to the third waveguide. (**b**) Calculated attenuation coefficient for each waveguide according to the method in[S3,S4]. The following relationships are used: the attenuation coefficient α = 4.34(ln$R$-lnR')/L, the end-face reflectivity $R=(n_{\mathrm{eff}}-1)^2/(n_{\mathrm{eff}}+1)^2$, the combined loss-reflection factor $R'=[1-(1-K^2)^{1/2}]/K$, and the contrast of the Fabry–Perot resonances $K=(I_{\max}-I_{\min})/(I_{\max}+I_{\min})$. Here, n_{eff} = 2.212 is the effective index at 1550 nm, L = 30 mm is the waveguide length, and $I_{\max}$ and $I_{\min}$ denote the peak and valley of the transmitted light intensity in a, respectively.

Section 4: Experimental details

A tunable linearly polarized Er-doped fiber laser at C-band (YO13040139, Yenista Inc., French), with a linewidth of 17 pm and a tuning range from 1546 to 1556 nm, was used to provide the signal wavelength, which was amplified by an all-fiber amplification stage to increase the signal power from 10 to 27.79 dBm (Fig. S3(a)). A fiber-coupled polarization-maintaining single-mode LD, with a maximum output power of 26.02 dBm at 973.85 nm was used as the pump source. The signal and pump lights were coupled with a wavelength division multiplexer before entering the fabricated few-mode PPLN waveguide. The layout of the light sources for SFG is displayed in Fig. 2(a). A bandpass filter was placed after the waveguide for filtering SFG light at 598 nm. The SFG power was measured with a power meter (3 A, Ophir Optronics Solutions, Ltd., Israel); the pump and SFG spectra by a spectral analyzer, with a spectral resolution of 0.02 nm (AQ6370D, Yokogawa Electric Corporation, Japan). To catch the spatial mode profile, a 20X object lens (Sigma Inc., Japan) was placed in front of the waveguide output surface (Fig. S3(b)). The spatial mode profile was measured using a CCD camera (COMS-1202, Cinogy Inc., Germany).

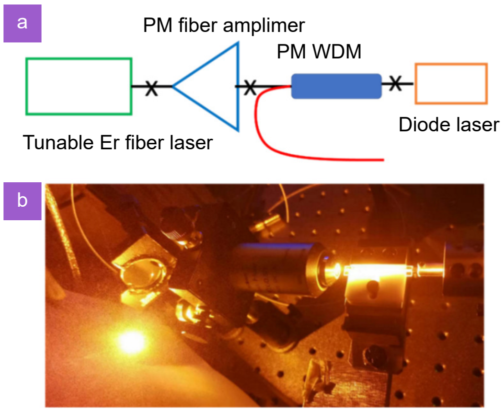

Fig. S3 | (**a**) Layout of the light source consisting of pump and signal lights; (**b**) image of the spatial mode steerable SFG experiment.

Section 5: Evaluating the coupling modes

In the two-mode coupling state between TM01 and TM10, we obtained the coupling mode matrix by varying r_1 from 0.1 to 3 with a step of 0.1 and varying θ1 from −π to π with a step of π/180. By matching the mode pattern in the matrix with a given coupling mode, that is, the patterns in Fig. 4(d), the relative amplitude and phase angle between TM01 and TM10 can be estimated. In the three-mode coupling state among TM01, TM10, and TM00, a primary pattern in the two-mode coupling matrix was selected to match the three-mode coupling pattern before sweeping the parameters between r_2 and θ_2 to simulate the three-mode coupling pattern (Table S5).

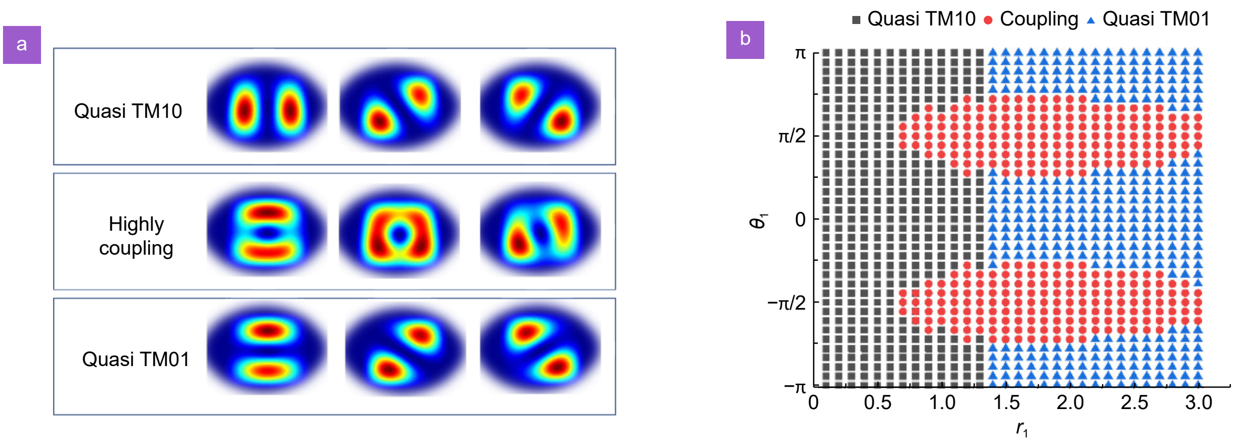

Fig. S4 | (**a**) Mode patterns classified as the quasi TM10, quasi TM01, and the high coupling modes; and (**b**) parameter range for the high coupling mode between TM10 and TM01.

Table S5 | Simulating the three-mode coupling process

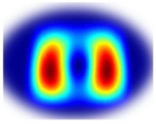	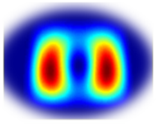	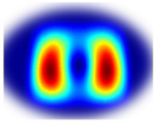	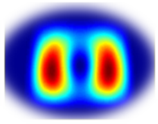	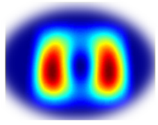
r_2=0.2, θ_2=−π	r_2=0.2, θ_2=−π/2	r_2=0.2, θ_2=0	r_2=0.2, θ_2=π/2	r_2=0.2, θ_2=π
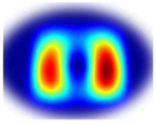	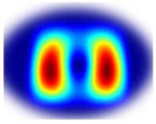	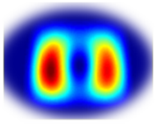	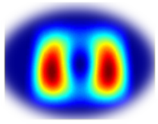	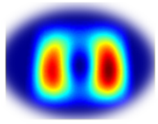
r_2=0.5, θ_2=−π	r_2=0.5, θ_2=−π/2	r_2=0.5, θ_2=0	r_2=0.5, θ_2=π/2	r_2=0.5, θ_2=π
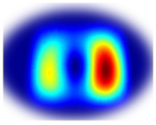	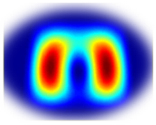	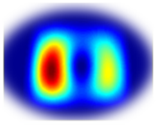	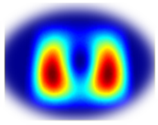	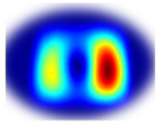
r_2=0.8, θ_2=−π	r_2=0.8, θ_2=−π/2	r_2=0.8, θ_2=0	r_2=0.8, θ_2=π/2	r_2=0.8, θ_2=π
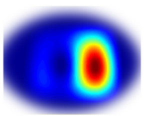	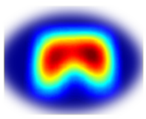	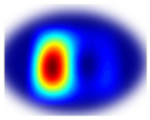	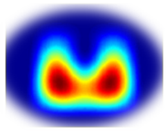	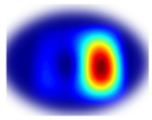
r_2=1.2, θ_2=−π	r_2=1.2, θ_2=−π/2	r_2=1.2, θ_2=0	r_2=1.2, θ_2=π/2	r_2=1.2, θ_2=π
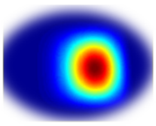	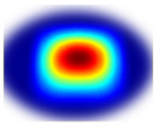	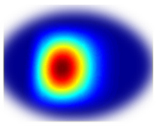	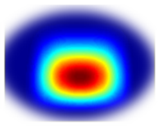	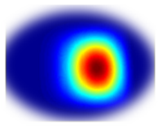
r_2=2.4, θ_2=−π	r_2=2.4, θ_2=−π/2	r_2=2.4, θ_2=0	r_2=2.4, θ_2=π/2	r_2=2.4, θ_2=π

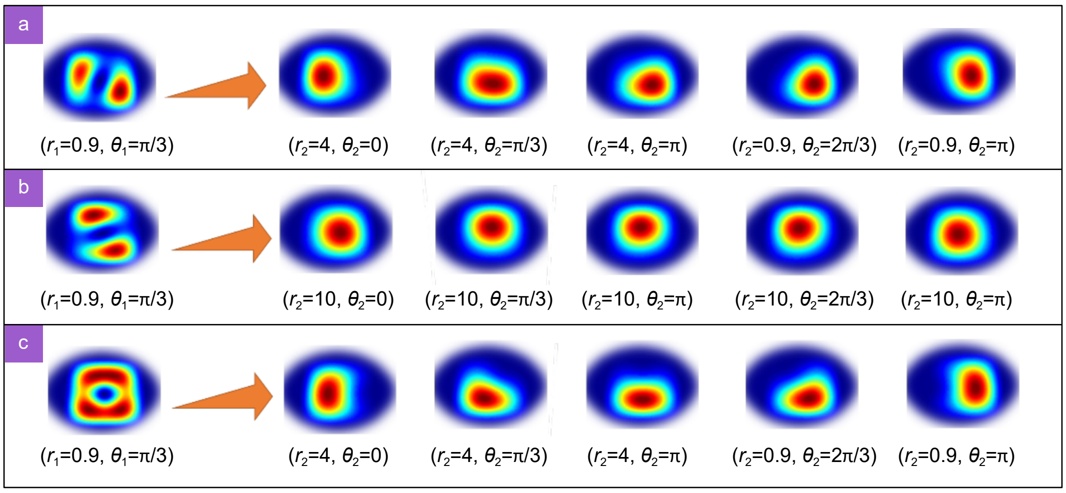

Fig. S5 | Three-mode coupling pattern under sufficiently high TM00 mode intensity for the initial (**a**) quasi TM01, (**b**) quasi TM10, and (**c**) highly coupling modes defined in Fig. S4.

Section 6: Wavelength-dependent spatial mode steering scheme

Table S6 | Evolution of the spatial mode in the wavelength-dependent spatial mode steering SFG scheme at 35°C

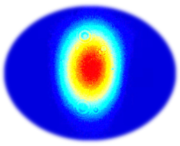	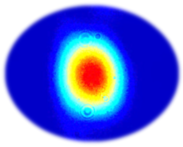	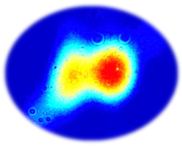	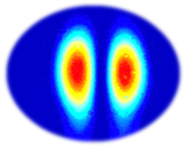
1546 nm	1548 nm	1549 nm	1550 nm
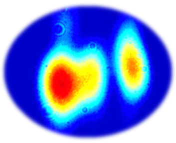	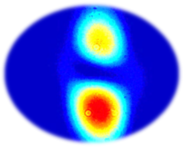	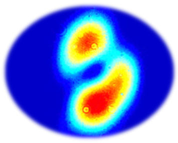	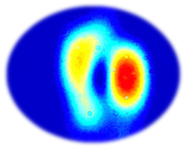
1556 nm	1554 nm	1553.3 nm	1553 nm

Table S7 | Evolution of the spatial mode in the wavelength-dependent spatial mode steering SFG scheme at 45°C

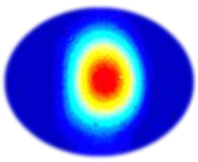	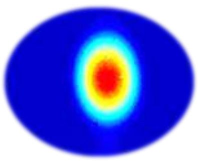	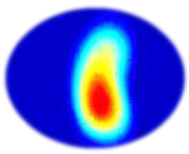	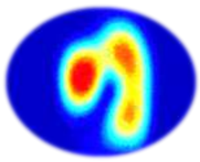
1546 nm	1551 nm	1552 nm	1553.6 nm
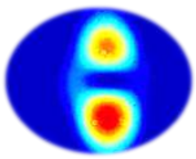	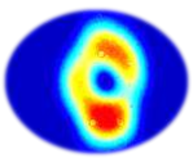	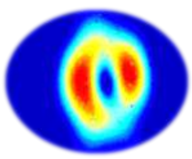	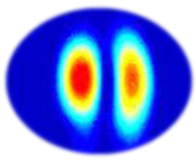
1556 nm	1555.7 nm	1555.3 nm	1554 nm

Table S8 | Evolution of the spatial mode in the wavelength-dependent spatial mode steering SFG scheme at 55°C

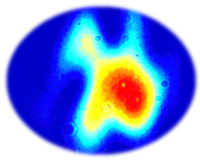	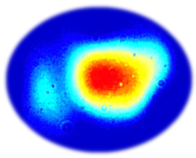	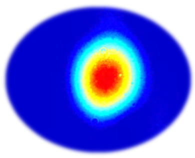	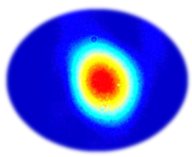
1546 nm	1547 nm	1548 nm	1550 nm
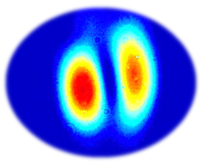	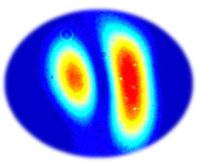	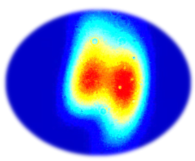	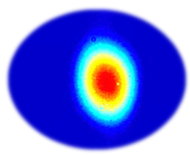
1556nm	1555 nm	1554 nm	1553 nm

Table S9 | Evolution of the spatial mode in the wavelength-dependent spatial-mode steering SFG scheme at 65°C

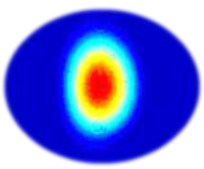	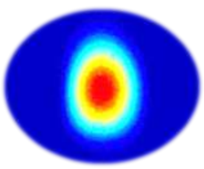	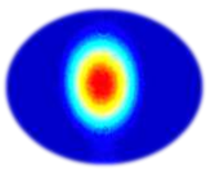	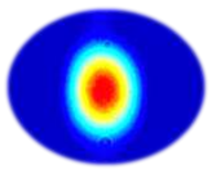
1546 nm	1549 nm	1553 nm	1556 nm

References

S1. Gayer O, Sacks Z, Galun E, Arie A. Temperature and wavelength dependent refractive index equations for MgO-doped congruent and stoichiometric $LiNbO_3$. *Appl Phys B* **91**, 343–348 (2008).

S2. Boyd R. *Nonlinear Optics* (Academic Press, 2008).

S3. Regener R, Sohler W. Loss in low-finesse Ti: $LiNbO_3$ optical waveguide resonators. *Appl Phys B* **36**, 143–147 (1985).

S4. Dong P, Qian W, Liao SR, Liang H, Kung CC et al. Low loss shallow-ridge silicon waveguides. *Opt Express* **18**, 14474–14479 (2010).